Effect of Surfactant on Retention Behaviors of Polystyrene Latex Particles in Sedimentation Field−Flow Fractionation: Effective Boundary Slip Model Approach

ARTICLE *in* LANGMUIR · JULY 2012

Impact Factor: 4.46 · DOI: 10.1021/la301593b · Source: PubMed

3 AUTHORS, INCLUDING:

Sun Tae Kim
Hannam University
15 PUBLICATIONS **89** CITATIONS
SEE PROFILE

Seungho Lee
Hannam University
63 PUBLICATIONS **535** CITATIONS
SEE PROFILE

Langmuir

Article

pubs.acs.org/Langmuir

Effect of Surfactant on Retention Behaviors of Polystyrene Latex Particles in Sedimentation Field-Flow Fractionation: Effective Boundary Slip Model Approach

Sun Tae Kim,[†] Kyunil Rah,[‡] and Seungho Lee*,[†]

[†]Department of Chemistry, Hannam University, Daejeon 305-811, South Korea

[‡]IT and Electronic Materials R&D, LG Chem. Research Park, 104-1 Moonji-dong, Daejeon, South Korea

Supporting Information

ABSTRACT: A retention theory in sedimentation field-flow fractionation (SdFFF) was developed by exploiting the effective slip boundary condition (BC) that allows a finite velocity for particles to have at the wall, thereby alleviating the limitations set by the no-slip BC constraint bound to the standard retention theory (SRT). This led to an expression for the retention ratio R as $R = (R_o + v^*_b)/(R_o + v^*_b)$, where R_o is the sterically corrected SRT retention ratio and v^*_b is the reduced boundary velocity. Then, v^*_b was modeled as $v^*_b = v^*_{b,o}/[1 + (7K^*S_o)^{1/2}]$, where S_o is the surfactant (FL-70) concentration and K^* is the distribution coefficient associated with the Langmuirian isotherm of the apparent effective mass against S_o. We applied this to study the surfactant effect on the retention behaviors of polystyrene (PS) latex beads of 170−500 nm in diameter. As a result, an empirical relation was found to hold between $v^*_{b,o}$ and d_o (estimated from R_o at $S_o = 0$) as $v^*_{b,o} - v^*_{o,o}[1 - (d_c/d_o)]$, where $v^*_{o,o}$ is the asymptotic value of $v^*_{b,o}$ in the vanishing d_c/d_o limit and d_c is the cutoff value at which $v^*_{b,o}$ would vanish. According to the present approach, the no-slip BC ($v^*_{b,o} = 0$) was predicted to recover when $d_o \sim d_c$, and the boundary slip effect could be significant for $S_o \leq 0.05\%$, particularly for large latex beads.

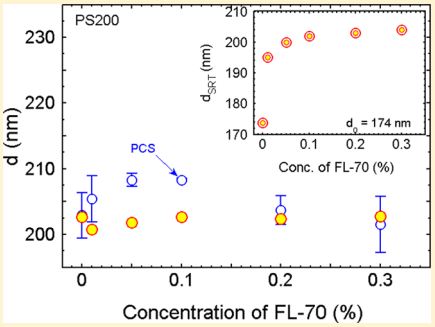

INTRODUCTION

The conventional parabolic flow profile for velocity with no-slip (stick) boundary condition (BC) embedded therein has long been invoked to explain[1] why large particles are easy to remove from a solid surface by blowing past the surface, but small particles are not. Indeed, this parabolic velocity profile has been applied with great success to model many macroscopic fluid flow experiments which would be insensitive to a partial-slip BC, mainly because of the large length scales of channel thickness compared to the slip length. Without fluid slip, Reynolds predicted a hydrodynamic force inversely proportional to the distance between the surfaces.[2,3] However, there are many cases for which the no-slip BC cannot account for the characteristic flow properties with sufficient accuracy, particularly for systems with large surface to volume ratio as in microfluidics and microelectro-mechanical systems (MEMS)[4,5] or with channel walls having very weak interactions with the (carrier) fluid itself or the relatively large (colloidal/polymer/biological) particles embedded therein via smooth channel surface[6−9] or highly water-repellent walls,[10] let alone for low-density gas flows in microchannels.[11] Those sizable deviations from the predictions based on the no-slip BC have spurred a number of studies on the limitations thereof, for instance, via apparent slip of particles at the wall[12,13] or models based on "drainage" experiments where there is a real slip for the fluid velocity at the wall.[6−10,14−22] For instance, recent studies on flow of Newtonian fluids demonstrated that the slip length is dependent upon the surface roughness,[6−9] the fluid−wall interactions,[16,17] the liquid viscosity and the shear rate,[22,23] and so forth, legitimately pondering the question of the generic validity of the explanations and predictions made on the tenet of the no-slip BC and parabolic velocity profile.

Field-flow fractionation (FFF) is a separation technique that is based on coupling of a laminar flow in a ribbon-like channel of $\sim 10^2$ μm thickness and an external field applied perpendicular to the flow direction,[24] and is useful for separation and characterization of colloidal particles,[25,26] polymers,[27,28] and biological macromolecules.[29,30] It has been demonstrated that sedimentation field-flow fractionation (SdFFF) not only separates colloidal particles at high levels of resolution, often for subsequent characterizations and analysis,[31] but also allows estimation of particle mass, hydrodynamic diameter, density, and related properties for various colloidal particles from the retention ratio determined from the measured elution volumes.[32−38] As for a theoretical basis to serve the purpose, a first-order retention theory has been developed[39] based upon a set of assumptions, such as an infinite parallel plate channel, a parabolic flow profile with no-slip BC for velocity, an equilibrium concentration distribution, uniform sedimentation forces, and the absence of extraneous

Received: April 19, 2012
Revised: June 11, 2012
Published: July 4, 2012

nonuniform forces. Clearly, the "standard" retention ratio expression derived thereby represents the retention behavior of an ideal system consisting of non-interacting "point" particles in order to make the theory tractable. Despite the set of ideal conditions upon which the standard retention theory (SRT) was built, its resulting retention ratio expression has been applied to account for the retention behaviors of many colloidal systems[35−38] with great success. This indicates that the primary features of the assumed ideal retention behaviors in SdFFF can be translated successfully into laboratory practice, in one way or another, so as to make the SRT applicable as widely as possible by effectively minimizing the perturbing effects which can potentially lead to nonideal retention behaviors.

Nevertheless, there have been an increasing number of cases in which departures from ideal retention behavior as described by the SRT are evident. And many theoretical and experimental efforts have been made to account for the discrepancies between the SRT and experiment by considering the corrections for the nonideal perturbations induced from, for instance, finite particle size effects due to steric exclusion at the walls,[40,41] nonequilibrium effects due to flow,[42] the presence of extraneous forces arising because of adsorption,[43,44] hydrodynamic lift forces, particularly, for large particles,[45−47] and the existence of the interactions between colloidal particles as well as between the particles and the channel surface,[48−50] to cite just a few. In this regard, it is quite likely that these perturbing forces influence the velocity profiles of colloidal particles, especially for large particles near the wall. For instance, we imagine a spherical latex particle with its bottom surface in contact with the wall. The particle will experience a different degree of dragging effect between its top and bottom parts owing to a velocity gradient developed in the flow because of the no-slip BC at the bottom wall. In light of the phenomenon that large particles are easier to remove from a solid surface by blowing past the surface than small ones, a large latex particle would be more subject to such disparity in the perturbing forces exerted by incessantly colliding molecules against it than a small particle. In any case, the circumstance will eventually end up as a hydrodynamic lifting effect (especially for large particles),[45−47] consequently giving rise to a slip at the boundary. The SRT as it stands, however, cannot take into consideration any explicit perturbations other than the steric exclusion effect as already accommodated in the sterically corrected retention ratio expression.[40]

Among such perturbing forces in SdFFF, the most crucial one is perhaps due to the wall effect attributed to the interactions existing between the latex particles and the channel surface. For a successful application of the SRT or its derivatives, therefore, an effective means is required that enables as little as possible overall wall effect so that the particles follow the presumed ideal retention behavior. For example, an introduction of appropriate additives into latex systems is one of the most frequently practiced prescriptions to control the retention/elution behavior of the particles in ordinary SdFFF operations. Such additives include surfactants, pH controllers, salts to adjust surface charges and ionic strengths, stabilizers, and so on. Thus, it is clear that the additives consequently affect the retention behavior of the particles by creating perturbing influences on the interactions between the particles and the channel wall.

Without loss of generality, the additive effect on the interactions between the particles and the channel wall can be interpreted in terms of attraction/repulsion of colloidal particles with the channel surface. Namely, while colloidal particles pass through the channel in SdFFF, there occurs competition between instant (dynamic) adsorption of the latex particles onto the channel surface and repulsion from the wall. On one hand, the dynamic adsorption of colloidal particles onto the channel surface generally decreases the particle elution velocities and the retention ratio, thereby resulting in an increased apparent hydrodynamic diameter when estimated from the SRT. On the other hand, repulsion of particles from the wall would accelerate the elution of particles out of the channel, giving rise to an increase in retention ratio, thereby a decrease in the apparent hydrodynamic diameter. Of course, the overall competition between the attractive (dynamic adsorption) and repulsive (dynamic desorption) forces depends on not only the nature of additives used, but also their concentrations: e.g., the size estimated from the SRT for a polystyrene (PS) latex solution tends to agree well with the nominal value when the concentration of a surfactant, say, FL-70, is about 0.1% or larger. Despite such a common practice in ordinary SdFFF operations, the precise physical mechanisms of such additive effects, especially on the retention behavior in SdFFF, are far from comprehensive and are open to further investigations, both experimentally and theoretically. Moreover, it remains as yet a scientific challenge to comprehend this additive effect to a molecular/particle level without undue complexity. In this work, we hope to address this problem by investigating the retention behaviors of polystyrene (PS) latex particles as a function of the surfactant concentration.

For the sake of simplicity, we focus our attention in this work on the wall effect, particularly as a function of the concentration of FL-70 added into PS latex systems. It is assumed that the concentration of the particles close to the wall can affect the local viscosity via hydrodynamic effects: For instance, a high enough concentration of the particles in contact with the bottom wall can increase the local (intrinsic) viscosity and thus slow down the flow velocity close to the wall. To this end, we will derive a generalized retention ratio expression in SdFFF by allowing a finite velocity for a flow including particles to have at the wall, thereby alleviating the limitations set by the no-slip BC constraint bound to the SRT. Basically, this approach enables us to get an insight into the importance of the mechanism of a possible transition from the slip to no-slip BC and vice versa depending on the surfactant concentration.

THEORY

Retention Ratio in SdFFF. When the particles approach very close to the channel wall, the excluded volume effect between the latex particles and the channel walls plays a dominant role, where the retention ratio can be expressed as[39]

$$R = \frac{\langle c(x)v(x)\rangle}{\langle c(x)\rangle\langle v(x)\rangle} = \frac{w\int_a^{w-a} c(x)v(x)\,\mathrm{d}x}{\int_a^{w-a} c(x)\,\mathrm{d}x\int_o^{w} v(x)\,\mathrm{d}x} \quad (1)$$

Here, $c(x)$ and $v(x)$ are the sample concentration and velocity profiles, respectively, expressed as a function of the channel thickness coordinate x, and w is the channel thickness and a is the measure of the excluded distance for latex particles from the wall. The angular brackets in eq 1 denote cross-sectional average. It is worthwhile to note that the retention ratio above is equivalent to the ratio of channel void volume V_o to retention volume V_r and it is this quantity $R = V_o/V_r$ that is measured in practice in most SdFFF experiments.

dx.doi.org/10.1021/la301593b | Langmuir 2012, 28, 10672−10681

The concentration profile $c(x)$ in eq 1 is postulated[31,49] to take the Boltzmann expression, $c(x) = c_o \exp[-V(x)/k_BT]$, where c_o is the concentration at a reference point and k_B and T are the Boltzmann constant and absolute temperature, respectively. $V(x)$ is the potential energy exerted on a particle of which the center of mass is at coordinate position x and can be split into two parts as $V(x) = V^{ext}(x) + V_p(x)$. Here, $V^{ext}(x)$ is the potential energy due to an external force applied to the system, for example, a centrifugal force

$$V^{ext}(x) = m_e G x \tag{2}$$

where

$$m_e = \frac{4}{3}\pi\left(\frac{d}{2}\right)^3(\rho_s - \rho) \tag{3}$$

is the effective mass (true mass minus buoyant mass) of spherical colloidal particles of diameter d and mass density ρ_s and ρ is the carrier liquid density (e.g., ρ_s = 1.05 g/mL for polystyrene and ρ = 1.00 g/mL for water), and G is the sedimentation field strength expressed as acceleration. The mean potential energy $V_p(x)$ is originated from the particle−particle and particle−wall interactions, being implicitly coarse-grained over an appropriate fluid volume (length scale) within which the particle of attention is under the mean-field forces exerted by the surrounding latex particles (including carrier molecules) and the channel walls.

As for $v(x)$, a parabolic flow profile under laminar flow condition is frequently taken as the simplest case to represent the velocity profile of a fluid consisting of the latex particles and carrier liquid molecules. However, as mentioned earlier, there are many cases showing a sizable deviation from the prediction of the characteristic flow properties made on the basis of the parabolic velocity profile. We will demonstrate in this work that this no-slip velocity profile tends to be valid when there is a high enough concentration of the colloidal particles in contact with the channel surface. To this end, we assume the velocity profile $v(x)$ as

$$v(x) = v_o(x) + v_b \tag{4}$$

where $v_o(x)$ is the parabolic velocity profile obeying the no-slip BC, i.e.,

$$v_o(x) = 6\langle v_o\rangle\left[\left(\frac{x}{w}\right) - \left(\frac{x}{w}\right)^2\right] \tag{5}$$

and $\langle v_o\rangle$ is the average flow velocity of $v_o(x)$. Basically, we have lifted the constraint of no-slip BC (i.e., $v_b = 0$) on which the SRT was built,[31] taking into consideration the possibility of a finite velocity for the flow to attain at the wall, namely, $v_b \geq 0$.

It should be noted that $v(x)$ stands for the velocity of the local flow consisting of the colloidal particles and the carrier liquid molecules, implying that the particle velocity can affect the carrier liquid velocity profile and vice versa. Furthermore, since the local flow viscosity or velocity can depend on the local particle concentration, particularly near the bottom wall, v_b may generally be a function of x, i.e., $v_b = v_b(x)$. However, an explicit description of v_b with respect to x constitutes a challenge beyond the present phenomenological approach taken in this work. For the sake of simplicity, we thus assume that v_b is independent of x and depends on the latex particle size, surfactant concentration (ionic strength), and so on, as detailed later in this work.

From eqs 1 and 4, it is straightforward to get a retention ratio expression as

$$R = \frac{R_o + v^*_b}{1 + v^*_b} \tag{6}$$

where v^*_b is the reduced boundary velocity defined as $v^*_b = v_b/\langle v_o(x)\rangle$. This v^*_b amounts to the relative velocity at the boundary (wall) with respect to the mean velocity of the no-slip case. It should be noted that eq 6 is exact as far as v_b is independent of x. The unperturbed retention ratio R_o in eq 6 is obtained from the no-slip boundary condition using $v_o(x)$, i.e., from eqs 4 and 6 as

$$R_o = 6(\alpha - \alpha^2) + 6\lambda(1 - 2\alpha)\left[\coth\left(\frac{1 - 2\alpha}{2\lambda}\right) - \frac{2\lambda}{(1 - 2\alpha)}\right] \tag{7}$$

with $\alpha = a/w = d/(2w)$ and the retention parameter λ is given by

$$\lambda = \frac{6k_BT}{\pi d^3(\rho_s - \rho)wG} = \frac{k_BT}{m_e wG} \tag{8}$$

Physically, λ is a measure of the strength of thermal energy relative to the energy required to drive a particle from $x = 0$ to $x = w$. By solving eq 6 for R_o, we get

$$R_o = R(1 + v^*_b) - v^*_b \tag{9}$$

which can be numerically solved to estimate m_e or d, provided that the information on R and v^*_b is available.

At this point, it is noteworthy that Williams et al.[49] have derived an approximate expression for R to accommodate the particle−wall interactions in terms of an empirical parameter δ_w serving as a measure of the "soft" exclusion layer, that is,

$$R = R_o\left(1 + \frac{\delta_w}{\lambda w}\right) \tag{10}$$

where $\delta_w = \int(1 - \exp[-\beta V(x)])\,dx$. To learn what physical insights and limitations eq 10 would have in explaining the surfactant effect on the retention behaviors in SdFFF, we have calculated δ_w/d as a function of ionic strength I (from S_o) for a given d value such that eq 10 is satisfied. As shown in Figure 1, the reduced soft exclusion layer thickness δ_w/d on I is pronounced, particularly for $I \leq 1.2 \times 10^{-4}$ (M) or $S_o \leq$ 0.1%. For a given PS latex, the maximum of δ_w/d occurs without exception when $S_o = 0$, indicating that the particles experience a mean field of repulsive forces from the wall to the maximum extent when $S_o = 0$. In general, repulsive forces are short-ranged so that they vanish within a distance of a few particle diameters. However, the max of δ_w/d for d = 170 nm, for instance, is about 9 at $S_o = 0$, much larger than a few diameters. Moreover, the dependence of δ_w/d on d is far from negligible, particularly for $I \leq 1.2 \times 10^{-4}$ (M). As shown in the inset, δ_w increases with d, implying that hydrodynamic lift forces[45−47] could exert a significant influence on the retention behaviors of the PS beads, especially when S_o is not high enough. Therefore, it should be useful to develop a physical model that helps us to better understand the surfactant effect on the retention behaviors of latex particles in SdFFF.

Model for Effective Boundary Velocity, v^*_b. In general, the reduced boundary velocity v^*_b may be a complex function

dx.doi.org/10.1021/la301593b | Langmuir 2012, 28, 10672−10681

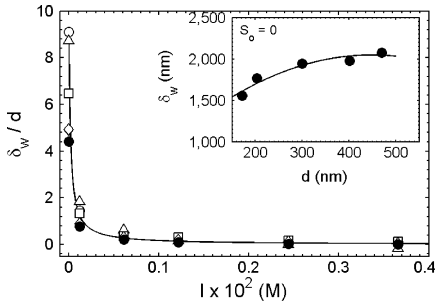

Figure 1. Dependence of reduced soft exclusion layer (δ_w/d) on ionic strength I for PS latex beads of various sizes. The open circles (○) are for d = 172 nm (PS170), triangles (Δ) for d = 202 nm (PS200), squares (□) for d = 300 nm (PS300), diamonds (◊) for d = 401 nm (PS400), and filled circles (●) for d = 470 nm (PS500), respectively. The solid line is a plot of $\delta_w/d = 8.7/(1 + 5I)$. In the inset, the soft exclusion layer thickness δ_w at $S_o = 0$ is plotted against the nominal diameter d_n of PS latex beads.

of the various properties of materials used. Since we do not have an available microscopic theory to take into consideration those properties, however, we will resort to a physical model for v^*_b. With this in mind, we pay a close attention on the slip model suggested by Myong[11] based on the Langmuir adsorption isotherm to study a pressure-driven microchannel gas flow. We will hinge upon the physical picture underlying this Langmuir adsorption slip model to construct a slip boundary velocity model for v^*_b, as detailed below.

While colloidal particles pass through the SdFFF channel, there occurs competition between the adsorption and desorption of the latex particles at the channel wall, for example, via van der Waals and/or electrostatic interactions. In this work, we will consider only dynamic (instant) and reversible particle−wall interactions, where the surfactant molecules are assumed to play a bridging role between the latex particles and the wall. To be specific, we consider a reversible ″simultaneous two-site″ (STS) adsorption of a single surfactant molecule onto both surfaces of a latex particle and the channel, ending up with a surfactant molecule occupying two adsorption sites of which one site is on a latex particle surface and the other on the channel surface. This STS adsorption is schematically illustrated in Figure 2, where the surfactant molecules within the dashed circle are bridging a latex particle and the wall, leading to an instant adsorption of a colloidal particle onto the channel surface, entailing a slowdown in the elution of the particles.

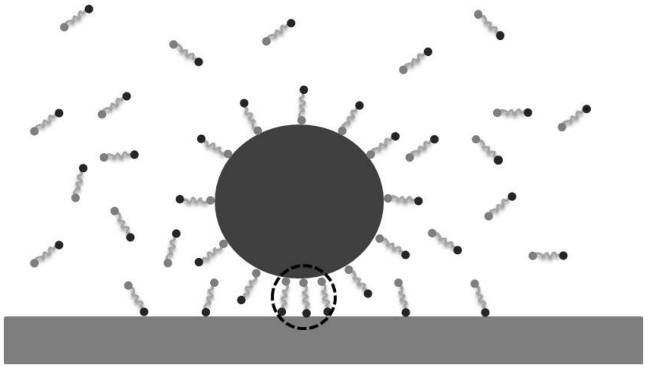

Figure 2. Schematic illustration of simultaneous two-site (STS) binding of surfactant molecules (in the dashed circle).

Let us denote X as the fraction of the adsorption sites occupied by surfactant molecules at thermal equilibrium. Those adsorption sites available on both surfaces of the particles and the wall are assumed to be indistinguishable from each other regardless of their accommodation preference to the ″head″ or ″tail″ of a surfactant molecule. Then, the probability that a particular surfactant molecule is adsorbed to an adsorption site on a particle is X, and the probability that the same molecule is adsorbed to an adsorption site on the wall is also X. Therefore, the probability of the two sites (from a particle and the wall) being simultaneously occupied by a single surfactant molecule to form a ″bridge″ is proportional to X^2. It is this reversible STS adsorption of surfactant molecules that practically leads to an adsorption of the colloidal particles onto the channel surface. This dynamic anchoring of the colloidal particles onto the channel surface via the bridges formed by surfactant molecules will reduce the probability for the particles to slip at the wall, entailing a slowdown in the elution of the particles. On the other hand, the probability of the two sites being unoccupied is proportional to $(1 - X)^2$, which represents the probability to keep the particles off the wall, leading to an accelerated elution.

The reason we are interested in the probability of $(1 - X)^2$ instead of $(1 - X)$ is as follows. The bridging lengths that the surfactant molecules can span could be around the minimum distance l_{min} by which the surface of a latex particle is separated from the channel surface. This suggests that, once a surfactant molecule is within the slab of $0 \le x \le l_{min}$ formed by a latex particle surface and the wall, both of its head and tail should simultaneously occupy two adsorption sites to form a bridge between them. Namely, for those sites available for STS adsorption within $0 \le x \le l_{min}$ (see the dashed circle in Figure 2), either both sites or none of them should be occupied at the same time with the probability of X^2 and $(1 - X)^2$, respectively.

The adsorption of colloidal particles onto the wall is presumed to be in dynamic equilibrium with their desorption from the wall, which can be expressed as $X^2 \propto (1 - X)^2 K^* S_o$ or

$$X^2 = \varepsilon(1 - X)^2 K^* S_o \tag{11}$$

where ε is a proportionality constant, which may depend on the comprising materials of the channel, and S_o has approximately replaced the equilibrium concentration. As described earlier, the surfactant molecules are presumed to facilitate the dynamic adsorption of the latex particles onto the wall via the STS adsorption mechanism. Therefore, the higher S_o is, the higher X^2 is. Here, $K^*(T)$ is the equilibrium constant that measures the distribution between the adsorbed and the desorbed particles at T. Because both X and $(1 - X)$ should be positive, we can obtain

$$X = (1 - X)\sqrt{\varepsilon K^* S_o} \tag{12}$$

which can be solved for X to give rise to $X = (\varepsilon K^* S_o)^{1/2}/[1 + (\varepsilon K^* S_o)^{1/2}]$.

Since those adsorption sites unoccupied by surfactant molecules would not reduce the probability for the particles to depart away from the wall, the probability for the particles to slip against the channel surface is proportional to $(1 - X)$, namely,

$$v^*_b = v^*_{b,0}(1 - X) = \frac{v^*_{b,0}}{1 + \sqrt{\varepsilon K^* S_o}} \tag{13}$$

where $v^*_{b,o}$ is the reduced (dimensionless) boundary velocity when $S_o = 0$, which will be treated as an adjustable parameter at

dx.doi.org/10.1021/la301593b | Langmuir 2012, 28, 10672−10681

the moment. As will be demonstrated, it is empirically found that a fixed value for ε (e.g., $\varepsilon = 7$) performs very well throughout all the PS latex systems studied in this work. Therefore, all that remains to determine in order to unambiguously describe v^*_b in eq 13 is K^*.

As discussed earlier, K^* should reflect the resulting balance between the adsorption-driving attractive and the desorption-driving repulsive forces as a function of S_o. From the viewpoint of SRT, the only physical quantity that can depend on S_o (or I) is the apparent effective mass m_e (eq 3) associated with λ in eq 8. In general, m_e tends to increase with the attractive particle−wall interaction, meaning that an increase in dynamic particle adsorption onto the wall will increase m_e or d. Since the probability X^2 tends to increase (see eq 11) with S_o, m_e should increase with S_o until saturated. We remark that an increase in m_e does not mean an actual increase in particle mass. It rather effectively measures the degree of the dynamic particle adsorption onto the wall as a function of S_o. On the other hand, $K^*(T)$ remains unchanged at constant T, since $K^*(T)$ is a function of T only and independent of S_o. On the basis of this reasoning, we assume that the variation in m_e with respect to S_o can be described by the Langmuir isotherm

$$\frac{m_e}{m_{e,o}} = 1 + \frac{bK^*S_o}{1 + K^*S_o} \tag{14}$$

Here, $m_{e,o}$ is m_e at $S_o = 0$ and b is the y-axis intercept in the fit of $(m_e/m_{e,o} - 1)^{-1}$ against $1/S_o$.

As shown in Figure 3, we have carried out a Langmuir isotherm fit of the relative effective mass $m_e/m_{e,o}$ against S_o in

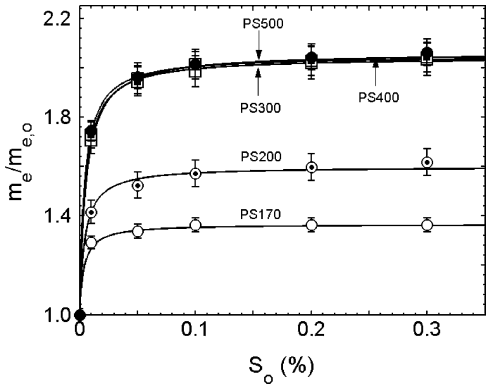

Figure 3. Langmuir isotherm fit (eq 14) of relative effective mass $m_e/m_{e,o}$ of PS latex beads against initial surfactant (FL-70) concentration S_o.

accordance with eq 14, where m_e is obtained from $R = R_o$. As a consequence, $m_e/m_{e,o}$ becomes almost saturated for $S_o \geq 0.1\%$ commonly for all the PS systems studied. The K^* and b values thus determined are summarized in Table 1, where K^* varies in the range of ca. 200 to 300, showing no strong dependence on the particle size. On the other hand, the parameter b turned out to increase with the particle size. This can be qualitatively understood in terms of the surface area of a latex bead onto which the number of binding sites available for the surfactant molecules increases in proportion to the PS bead size.

EXPERIMENTAL SECTION

Materials. Polystyrene latex standards having nominal diameters of 170, 200, 300, and 400 nm were purchased from Duke Scientific Corp. (Palo Alto, CA, USA), 500 nm from Fluka AG (Fluka Corp., Steinheim, Germany). The nominal diameter values d_n for the standard PS latex employed are indicated in Table 1 with the uncertainties associated therewith. It is presumed that the density of PS latex standard is 1.05 g/mL. The carrier liquid was water containing FL-70 of various concentrations (Fisher Scientific, Fair Lawn, NJ, USA).

Table 1. Nominal PS Latex Beads Diameters (d_n), and d_o and d Estimated at $S_o = 0$ from $R_o = R$ and eq 6, Respectively

latex	d_n (nm)	d_o[a] (nm)	d[b] (nm)	K^*[c] (%$^{-1}$)	b[c]	v^*_b
PS170	170 ± 5	154.2 ± 1.1	172.5	273	0.336	0.100
PS200	200 ± 6	173.7 ± 2.0	202.6	222	0.600	0.110
PS300	300 ± 9	234.5 ± 2.5	300.9	208	1.04	0.115
PS400	400 ± 12	313.4 ± 3.1	402.7	227	1.05	0.119
PS500	485 ± 24	368.8 ± 3.1	482.5	180	1.06	0.129

[a]Estimated from $R = R_o$ using eq 7. [b]From eq 6. [c]From Langmuir isotherm (Figure 3).

Sedimentation Field-Flow Fractionation (SdFFF). The sedimentation field-flow fractionation system used in this work has been described elsewhere.[26] The SdFFF channel used is 0.0127 cm thick, 89.1 cm long, and 1.1 cm wide. The radius of the channel rotor is 15.1 cm. The channel surface was polished Hastelloy-C which consists of Ni (56%), Mo (17%), Cr (15%), Fe (5%), W (4%), and traces of Mn, Si, and others. The channel void volume was measured from the elution volume of acetone to be 1.333 mL. The carrier solution was pumped by Futecs P-4000 Solvent Delivery Pump (Daejeon, Korea). The flow rate was measured by an Optiflow 1000 Liquid flowmeter (Agilent Technologies, Palo Alto, USA). The eluted particles were monitored by a UV-106 UV/vis detector (Linear Instruments, Reno, USA) operating at the fixed wavelength of 254 nm. The control of SdFFF operation and data collection/processing was performed by a personal computer loaded with the software provided by Postnova USA (Salt Lake City, Utah, USA). A 20 μL sample was injected into channel directly through a septum by use of microsyringe. All experiments were performed at room temperature.

Photon Correlation Spectroscopy (PCS). The sizes of PS beads were measured by a Nanotrac NPA 150 (Microtrac Inc., Nikkiso, Japan) which uses a 4 mW He−Ne laser (632.8 nm) as the light source. Experimental parameters were as follows: temperature 25 °C, viscosity 0.8460 cP, refractive index 1.333, and collection angle 90°. All measurements were repeated three times.

RESULTS AND DISCUSSION

In order to unambiguously describe the effective boundary slip velocity in eq 13, we need information on $v^*_{b,o}$, ε, and K^*. For the proportionality constant ε, it was found that a single value of $\varepsilon = 7$ performs well for all PS latex systems studied in this paper, as shown in Figures 4−. The distribution coefficient K^* has been systematically determined from the Langmuir isotherm fit of $m_e/m_{e,o}$ against S_o, as shown in Figure 3.

Since we do not have a molecular theory available for the reduced boundary velocity at $S_o = 0$, as denoted by $v^*_{b,o}$ in eq 13, it will be treated at the moment as an adjustable parameter by assuming that, when $S_o > 0.1\%$, the apparent diameter of d_{SRT} determined from the SRT (i.e., $R_o = R$) is accurate enough and the surfactant can suppress the particle−wall repulsions to the extent that the no-slip BC is obeyed. In other words, a value for $v^*_{b,o}$ is determined in such a way that the hydrodynamic diameter d at $S_o = 0$ obtained by solving $R_o = R(1 + v^*_{b,o}) - v^*_{b,o}$ agrees well with the asymptotic d value that attains as S_o increases to be larger than, say, 0.1%.

As a result, it has been found that $v^*_{b,o} = 0.100$ for PS170, 0.110 for PS200, 0.115 for PS300, 0.119 for PS400, and 0.130 for PS500 can account for the effective slip when $S_o = 0$. As a

dx.doi.org/10.1021/la301593b | Langmuir 2012, 28, 10672−10681

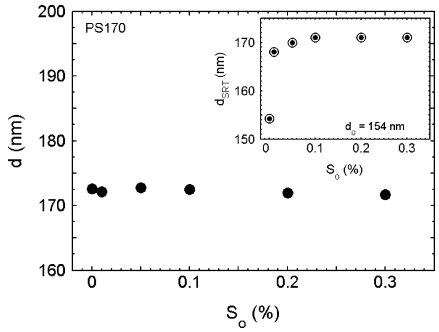

Figure 4. Hydrodynamic diameter d (filled circles) determined from eq 9 for PS170 with respect to surfactant (FL-70) concentration S_o. The double circles (⊙) in the inset are d_{SRT} determined under the no-slip boundary condition ($\nu^*_b = 0$).

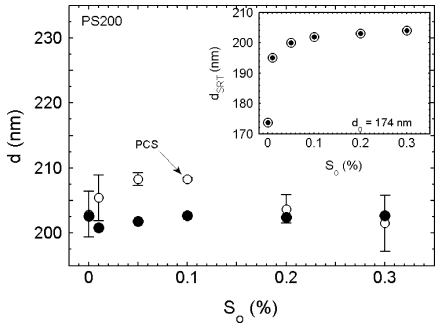

Figure 5. Hydrodynamic diameter d (filled circles) determined from eq 9 for PS200 with respect to surfactant (FL-70) concentration S_o. Open circles (○) are PCS results and the double circles (⊙) in the inset are d_{SRT} determined under $\nu^*_b = 0$.

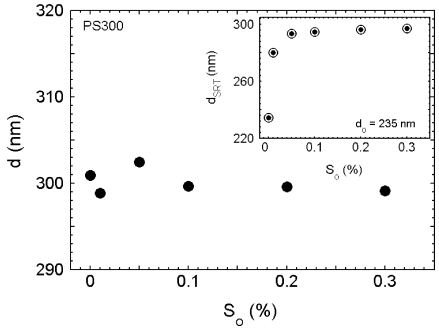

Figure 6. Hydrodynamic diameter d (filled circles) determined from eq 9 for PS300 with respect to surfactant (FL-70) concentration S_o. The double circles (⊙) in the inset are d_{SRT} determined under the no-slip boundary condition ($\nu^*_b = 0$).

matter of fact, as shown in Figure 9 and eq 16, it is intriguing to find an apparently excellent correlation between $\nu^*_{b,o}$ and (d_c/d_o), where d_c is a cutoff value at which $\nu^*_{b,o}$ vanishes so as to retain the effective no-slip BC, that is, $\nu^*_{b,o}(d_c) = 0$. Some important implications that this correlation suggests will be discussed below in more detail.

On the basis of eq 13 with $\nu^*_{b,o}$ and K^* values determined, respectively, the hydrodynamic diameters of the respective PS latex beads have been estimated as a function of the FL-70 concentration in Figures 5−9, respectively, for PS170, PS200, PS300, PS400, and PS500.

In Figure 4, we have estimated the hydrodynamic diameters d (filled circles) for the PS170 latex system as a function of S_o

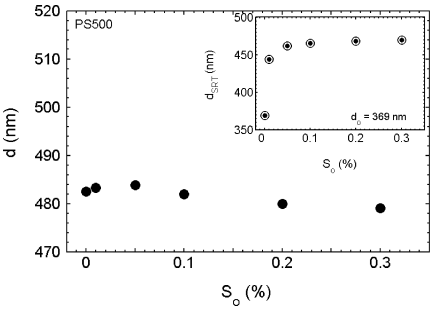

Figure 7. Hydrodynamic diameter d (filled circles) determined from eq 9 for PS400 with respect to surfactant (FL-70) concentration S_o. The double circles (⊙) in the inset are d_{SRT} determined under the no-slip boundary condition ($\nu^*_b = 0$).

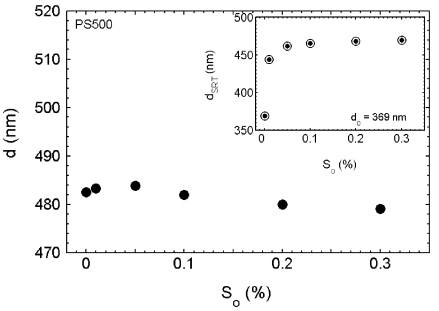

Figure 8. Hydrodynamic diameter d (filled circles) determined from eq 9 for PS500 with respect to surfactant (FL-70) concentration S_o. The double circles (⊙) in the inset are d_{SRT} determined under the no-slip boundary condition ($\nu^*_b = 0$).

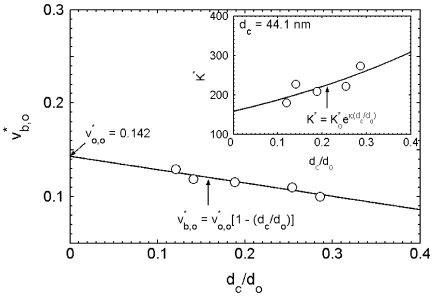

Figure 9. Correlation between the reduced effective boundary velocity $\nu^*_{b,o}$ at $S_o = 0$ and (d_c/d_o). Open circles in the inset are K^* values determined by fitting in Figure 1 and the line is a plot of $K^* = K^*_o \exp[\kappa(d_c/d_o)]$.

(%). The hydrodynamic diameters were calculated from eq 9 with the measured R (Table 2) and $\nu^*_b = \nu^*_{b,o}/[1 + (7K^*S_o)]$, where $\nu^*_{b,o} = 0.100$ and $K^* = 273$ (Figure 3). The estimated hydrodynamic diameter is 172.5 nm, which agrees remarkably well with the nominal value of 170 ± 5.0 nm (Table 1). In the inset, the double circles (⊙) were estimated under the no-slip boundary condition (i.e., $\nu^*_b = 0$) using $R = R_o$, where R_o is given by eq 7. The indicated $d_o = d_{SRT}$ $(S_o = 0) = 154$ nm is the specific d_{SRT} value when $S_o = 0$, which is in stark contrast to $d = 173$ nm estimated under the partial slip BC of $\nu^*_{b,o} = 0.100$. This indicates that the dynamic desorption-deriving repulsive forces are apparently dominant in the particle−wall interactions in pure water, leading to a partial boundary slip of $\nu^*_{b,o} = 0.100$. Obviously, ν^*_b decays rapidly to a very small asymptotic value as S_o increases from zero to, say, 0.1% or so, implying that addition of enough FL-70 facilitates the instant (dynamic)

dx.doi.org/10.1021/la301593b | Langmuir 2012, 28, 10672−10681

Table 2. Experimental Retention Ratio R and Diameters Determined for PS Beads at Various Surfactant Concentration S_o[a]

latex	S_o (%)	R	d_o[b] (nm)	d[c] (nm)	d_{PCS}[d] (nm)
PS170	0.00	0.2652	154	173	-
	0.01	0.2077	168	172	-
	0.05	0.1984	170	173	-
	0.10	0.1974	171	172	-
	0.20	0.1974	171	172	-
	0.30	0.1974	171	171	-
PS200	0.00	0.2276	174	203	202.9 ± 3.5
	0.01	0.1649	195	201	205.4 ± 3.5
	0.05	0.1538	200	202	208.3 ± 1.0
	0.10	0.1495	202	203	208.3 ± 0.2
	0.20	0.1481	203	202	203.7 ± 2.2
	0.30	0.1466	204	203	201.5 ± 4.3
PS300	0.00	0.1893	235	300	328.7 ± 0.5
	0.01	0.1185	280	299	299.2 ± 1.9
	0.05	0.1052	293	302	299.3 ± 0.9
	0.10	0.1046	295	300	291.8 ± 3.6
	0.20	0.1025	296	300	305.3 ± 0.6
	0.30	0.1019	297	299	283.4 ± 0.5
PS400	0.00	0.1944	313	403	-
	0.01	0.1203	380	402	-
	0.05	0.1096	392	403	-
	0.10	0.1073	396	402	-
	0.20	0.1060	397	400	-
	0.30	0.1046	398	401	-
PS500	0.00	0.2424	341	481	499.3 ± 1.5
	0.01	0.1311	432	484	445.3 ± 2.1
	0.05	0.1203	449	476	456.3 ± 3.8
	0.10	0.1159	457	476	462.3 ± 1.5
	0.20	0.1134	460	475	460.0 ± 1.7
	0.30	0.1119	461	475	447.3 ± 1.5

[a]The angular velocity was 2063, 1875, 1315, 846, and 658 rpm for PS170, PS200, PS300, PS400, and PS500, respectively. [b]Estimated from $R = R_o$. [c]From eq 6. [d]Data from PCS.

adsorption of the particles onto the wall via the bridging effects of the surfactant molecules to the extent that the no-slip BC virtually works to a good approximation. The resulting d estimated for PS170 employing eq 13 with $\nu^*_{b,o} = 0.100$ and $K^* = 273$ (Figure 3) remains virtually invariant as $d = 172 \pm 1.0$ nm with respect to S_o, validating the STS adsorption as a plausible mechanism to derive the dynamic particle adsorption onto the wall such that ν^*_b slows down with increasing S_o.

In Figure 5, the hydrodynamic diameters d (filled circles) were estimated for PS200 with respect to S_o (%) in the same way as was done in Figure 4. The open circles (○) were estimated employing a PCS technique, and the error bars are for the uncertainties associated therewith. In the inset, d_{SRT} values were from $R_o = R$ and $d_o = 174$ nm.

The PCS results marked by the open circles (○) in Figure 5 tend to increase to about 208 nm for S_o up to about 0.1%, from which they start declining to 202 nm upon increasing S_o to 0.3%. This qualitative trend of d_{PCS} against S_o can also be observed in the PS300 and PS500 latex systems (Table 2) with few exceptions. It is rather counterintuitive, however, to show a decrease in d_{PCS} with S_o, especially from the viewpoint that the higher the adsorbate (surfactant) concentration is, the greater the adsorption of the adsorbate onto the adsorbent, because this would normally result in an increase in the hydrodynamic diameter. In that regard, it may be useful to note that estimating d_{PCS} relies on the Stokes−Einstein relation

$$d_{PCS} = \frac{k_B T}{3\pi\eta D_{PCS}} \tag{15}$$

where η is the viscosity of the solvent and D_{PCS} is the Fickian diffusion coefficient of the particle determined by means of PCS from the Lorentzian-shape spectrum of the scattered radiation due to the thermal motion of the scattering particles. Therefore, decreasing d_{PCS} with S_o means most likely that D_{PCS} increases with S_o. Since there is no wall effect in a PCS experiment, the variations of D_{PCS} depend mostly on the particle−particle interactions as a function of S_o, although the Stokes−Einstein relation in eq 15 is strictly valid only for a relatively large sphere in a medium (solvent) where the concentration is very dilute to the extent that the interparticle interactions are totally negligible. This suggests that S_o larger than about 0.1% somehow causes an acceleration of the diffusion of the particles, which would usually come about under the circumstances where the interparticle repulsive interactions are increased due to Coulomb interactions between same surface charges, for example. In contrast to those PCS results, the hydrodynamic diameter estimated from eq 9 with $\nu^*_b = \nu^*_{b,o}/[1 + (7K^*S_o)^{1/2}]$ remains as $d = 202.3 \pm 0.8$ nm, showing almost no changes within the experimental variations of S_o.

In Figure 6, we have determined the hydrodynamic diameter d (filled circles) for the PS300 latex system with respect to S_o (%), where d is in the range of 300.2 ± 1.2 nm, independent of S_o, which are in excellent agreement with $d_n = 300 \pm 9$ nm, whereas in the inset, those estimated with no-slip BC (d_{SRT}) are underestimated by far when $S_o < 0.1\%$, where $d_o = 235$ nm.

In Figure 7, the hydrodynamic diameters d were estimated for the PS400 latex system as a function of S_o. The estimated d values are in the range of 401.8 ± 1.2 nm, which is in good agreement with $d_n = 400 \pm 12$ nm. The double circles (⊙) in the inset were for d_{SRT}.

As shown in Figure 8 for PS500, the average d value over the entire S_o range is 481.8 ± 1.9 nm in good agreement with $d_n = 485 \pm 24$, given the uncertainty associated therewith. The d_{SRT} values show somewhat sizable deviations from d_n when $S_o < 0.1\%$, where $d_o = 369$ nm. This suggests that the ideal retention behaviors assumed in the derivation of the SRT expression (eq 7) are not realized in the case of $S_o < 0.1\%$.

We have thus far adjusted $\nu^*_{b,o}$ in such a way that the d value when $S_o = 0$ as estimated from eq 6 would agree well with the saturated d_o value that is attained at $S_o \geq 0.1\%$. Intriguingly, however, an excellent correlation was found, as shown in Figure 9, between $\nu^*_{b,o}$ and (d_c/d_o) as

$$\nu^*_{b,o} = \nu^*_{o,o}\left[1 - \left(\frac{d_c}{d_o}\right)\right] \tag{16}$$

where $\nu^*_{b,o} = 0.142$ is the asymptotic value of $\nu^*_{b,o}$ in the vanishing (d_c/d_o) limit, $d_c = 41.1$ nm is the cutoff d_o value at which $\nu^*_{b,o}$ is predicted to vanish. Here, $\nu^*_{o,o} = 0.142$ is corresponding to the limiting maximum for $\nu^*_{b,o}$, and $d_c = 41.1$ nm may be considered as the limiting d_o value at which the no-slip BC may come to practically hold to a good approximation. In the inset, we have fitted K^* determined from Figure 3 into the form $K^* = K^*_o \exp[\kappa(d_c/d_o)]$, where $K^*_o = 158$ and $\kappa = 1.67$. There appears to be a reasonable correlation between K^* and (d_c/d_o).

dx.doi.org/10.1021/la301593b | Langmuir 2012, 28, 10672−10681

An implication of importance from the present approach is that the particle diameter can be estimated from $R_o = R(1 + \nu^*_b) - \nu^*_b$ with $\nu^*_{b,o} = \nu^*_{o,o}[1 - (d_c/d_o)]$, given that d_o is available from $R_o = R$. In Figure 10, we have calculated the

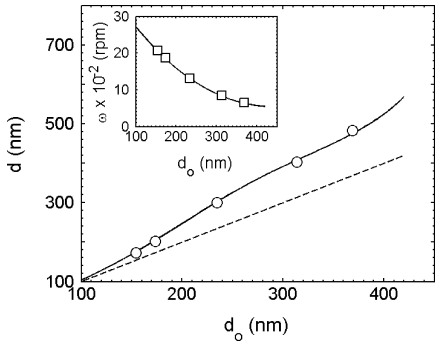

Figure 10. Plot of hydrodynamic diameter d (open circles) determined from eq 9 versus d_o estimated at $S_o = 0$. The open squares (□) in the inset are angular velocity ω used for the calculation of the diameters. The solid curve was calculated using ω given by the solid curve in the inset and the dashed curve (---) represents the $d = d_o$ case.

hydrodynamic diameters d in pure water using $R_o = R(1 + \nu^*_b) - \nu^*_b$ with $\nu^*_{b,o} = \nu^*_{o,o}[1 - (d_c/d_o)]$, where the open circles (○) are for those calculated, and the open squares (□) in the inset are the angular velocity ω used to measure R. The solid curve is calculated using ω given by the solid curve in the inset. For the sake of comparison, we have shown as well the ideal case of $d = d_o$ as marked by the dashed curve (---), where it shows sizable deviations from the open circles or the solid curve as d_o gets larger than approximately 100 nm. It should be pointed out that the extrapolated portion of the solid curve beyond $d_o = d_{SRT}(S_o = 0) = 369$ nm, which corresponds to the case of PS500, tends to show a high sensitivity to the angular velocity used for the calculation and should thus be taken with a grain of salt. Perhaps it is worthwhile to mention also that an unrealistic value of ω as an input for a given d_o value is prone to no converging solution to eq 9.

CONCLUSIONS

In the present paper, we have developed a retention theory in SdFFF by exploiting the slip boundary condition that allows a finite velocity for particles to have at the wall in the case of very low surfactant concentration. In this way, we have been able to alleviate the limitations set by the no-slip BC constraint (i.e., parabolic flow velocity profile) bound to the standard retention theory, thereby obtaining $R_o = (R_o + \nu^*_b) - (1 + \nu^*_b)$, where R_o is given by eq 7 and ν^*_b is the reduced effective boundary velocity. This ν^*_b represents the tendency of the dynamic desorption of the particles from the walls owing to the net repulsive forces of the particle−wall interactions, ending up with higher velocity states and thereby less retention than predicted by the SRT.

By hinging upon the mechanism of the "simultaneous two-site" (STS) adsorption of surfactant molecules, we have modeled the effective slip boundary velocity ν^*_b as $\nu^*_b = \nu^*_{b,o}/[1 + (7K^*S_o)^{1/2}]$. The distribution coefficient K^* is determined from the Langmuirian adsorption isotherm of the apparent effective mass m_e against S_o (Figure 3) that measures the degree of dynamic adsorption of the particles onto the channel surface via the STS adsorption mechanism mediated by additives such as surfactants. We have then applied this to study the surfactant effect on the retention behaviors of polystyrene latex beads of ca. 170 nm, 200 nm, 300 nm, 400 nm, and 500 nm, respectively, by calculating the hydrodynamic diameters of the latex particles as a function of FL-70 concentration from $R_o = R(1 + \nu^*_b) - \nu^*_b$, where R is measured by SdFFF.

As a result, the boundary slip effect was found to be significant in the case of $S_o \leq 0.05\%$, particularly for large beads. This suggests that the desorption-deriving repulsive forces play a dominant role in dictating the elution behaviors of the latex particles through the channel when $S_o \leq 0.05\%$. Addition of sufficient FL-70, on the other hand, enables the particle−wall repulsive forces to be overcome, entailing the no-slip boundary condition which effectively realizes the ideal retention behaviors of the latex particles that the SRT assumes as its tenet to derive eq 7.

An intriguing finding may be the relation empirically found to hold between $\nu^*_{b,o}$ and d_o as $\nu^*_{b,o} = \nu^*_{o,o}[1 - (d_c/d_o)]$, where $\nu^*_{b,o} = 0.142$ is the asymptotic value of $\nu^*_{b,o}$ for large particles in the vanishing (d_c/d_o) limit, $d_c = 41.1$ nm is the cutoff d_o value at which $\nu^*_{b,o}$ would vanish, respectively. We believe that the validity of this prediction for the no-slip BC to occur in the case of $d \approx d_c$ for PS latex beads constitutes an interesting investigation to carry out in further studies. It should be also interesting to verify an existence of d_c for other systems than PS beads, such as surface-modified PS beads, biomolecules, dendrimers, metallic nanoparticles, and so forth.

It is perhaps noteworthy that the dependence of ν^*_b on S_o as in eq 13 may provide a potential connection to the ionic strength of the suspending medium: $I = 1/2\Sigma_i c_i z_i^2$, where c_i is the bulk solution concentration of ionic species i and z_i is its charge. For the PS latex systems investigated, the ionic strength is proportional to S_o, i.e., $I \propto S_o$. Thus, it is possible to formally write the above expression for ν^*_b as a function of the ionic strength as

$$\nu^*_b = \frac{\nu^*_{b,o}}{1 + \chi\sqrt{I}} \tag{17}$$

where χ^{-2} is the ionic strength of an appropriate reference system. However, it is not clear at the moment whether or not an addition of salts instead of surfactants so as to control the ionic strength[52] would exert an influence on the effective boundary velocity ν^*_b in eq 13 in the same manner as that of a surfactant. We believe that an investigation of its dependence on the nature of additives such as surfactants or salts would be worthwhile to pursue in the future.

We remark that the overall particle−wall interactions, be they repulsive or attractive, are prone to depend on the channel wall materials. It is thus worthwhile to systematically examine the dependence of the retention behaviors of various latex beads including surface-modified latex beads on the channel wall materials (e.g., stainless steel, Teflon, polyimide) as well as on the nature of additives used such as surfactants (e.g., FL-70, SDS, Triton X-100), salts (e.g., NaN_3, $NaNO_3$, NaCl, etc.), pH controllers, and so on. It should also be interesting to investigate the adsorption effect[53] of very high polymers, proteins, and other organic materials on the retention behaviors of latex particles and their hydrodynamic sizes estimated therefrom.

dx.doi.org/10.1021/la301593b | Langmuir 2012, 28, 10672−10681

■ ASSOCIATED CONTENT

Supporting Information

SdFFF fractograms. This material is available free of charge via the Internet at http://pubs.acs.org.

■ AUTHOR INFORMATION

Corresponding Author

*Tel +82-42-629-8822. Fax +82-42-629-8811. E-mail: slee@hannam.kr.

Notes

The authors declare no competing financial interest.

■ ACKNOWLEDGMENTS

Authors acknowledge support by Hannam University. This research was also supported by Basic Science Research Program through the National Research Foundation of Korea (NRF) funded by the Ministry of Education, Science and Technology (2010-0003133).

■ REFERENCES

(1) Feynman, R. P.; Leighton, R. B.; Sands, M. *The Feynman Lectures on Physics*; Addison-Wesley: New York, 1965; Vol. *II*, p 41−1.

(2) Reynolds, O. On the theory of lubrication and its application to Mr. Beauchamp Tower's experiments, including an experimental determination of the viscosity of olive oil. *Philos. Trans. R. Soc. London* **1886**, *177*, 157−234.

(3) Reynolds, O. On the theory of lubrication and its application to Mr. Beauchamp Tower's experiments, including an experimental determination of the viscosity of olive oil. *Proc. R. Soc. London* **1886**, *40*, 191−203.

(4) Ho, C. M.; Tai, Y. C. Micro-electro-mechanical-systems (MEMS) and fluid flows. *Annu. Rev. Fluid. Mech.* **1998**, *30*, 579−612.

(5) Harley, J. C.; Huang, Y.; Bau, H. H.; Zemel, J. N. Gas flow in micro-channels. *J. Fluid Mech.* **1995**, *284*, 257−274.

(6) Zhu, Y.; Granick, S. Rate-dependent slip of Newtonian liquid at smooth surfaces. *Phys. Rev. Lett.* **2001**, *87* (9), 961051−961054.

(7) Zhu, Y.; Granick, S. Limits of the hydrodynamic no-slip boundary condition. *Phys. Rev. Lett.* **2002**, *88* (10), 1061021−1061024.

(8) Zhu, Y.; Granick, S. Reassessment of Solidification in Fluids Confined between Mica Sheets. *Langmuir* **2003**, *19* (20), 8148−8151.

(9) Cottin-Bizonne, C.; Cross, B.; Steinberger, A.; Charlaix, E. Boundary slip on smooth hydrophobic surfaces: Intrinsic effects and possible artifacts. *Phys. Rev. Lett.* **2005**, *94*, 5.

(10) Watanabe, K.; Udagawa, Y.; Mizunuma, H. Slip of Newtonian fluids at slip boundary. *J. Fluid Mech.* **1999**, *381*, 225−238.

(11) Myong, R. S. Gaseous slip models based on the Langmuir adsorption isotherm. *Phys. Fluids* **2004**, *16* (1), 104−117.

(12) Barnes, H. A. A review of the slip (wall depletion) of polymer solutions, emulsions and particle suspensions in viscometers: its cause, character, and cure. *J. Non-Newton. Fluid.* **1995**, *56* (3), 221−251.

(13) Denn, M. M. Issues in viscoelastic fluid mechanics. *Annu. Rev. Fluid. Mech.* **1990**, *22* (1), 13−34.

(14) Brenner, H. The slow motion of a sphere through a viscous fluid towards a plane surface. *Chem. Eng. Sci.* **1961**, *16* (3−4), 242−251.

(15) Maude, A. D. End effects in a falling-sphere viscometer. *Brit. J. Appl. Phys.* **1961**, *12* (6), 293−295.

(16) Ruckenstein, E.; Rajora, P. On the no-slip boundary condition of hydrodynamics. *J. Colloid Interface Sci.* **1983**, *96* (2), 488−491.

(17) Churaev, N. V.; Sobolev, V. D.; Somov, A. N. Slippage of liquids over lyophobic solid surfaces. *J. Colloid Interface Sci.* **1984**, *97* (2), 574−581.

(18) Chan, D. Y. C.; Horn, R. G. The drainage of thin liquid films between solid surfaces. *J. Chem. Phys.* **1985**, *83* (10), 5311−5324.

(19) Vinogradova, O. I. Drainage of a thin liquid film confined between hydrophobic surfaces. *Langmuir* **1995**, *11* (6), 2213−2220.

(20) Vinogradova, O. I. Hydrodynamic interaction of curved bodies allowing slip on their surfaces. *Langmuir* **1996**, *12* (24), 5963−5968.

(21) Vinogradova, O. I. Implications of hydrophobic slippage for the dynamic measurements of hydrophobic forces. *Langmuir* **1998**, *14* (10), 2827−2837.

(22) Craig, V. S. J.; Neto, C.; Williams, D. R. M. Shear-dependent boundary slip in an aqueous Newtonian liquid. *Phys. Rev. Lett.* **2001**, *87* (5), 054504/1−054504/4.

(23) Hoyos, M.; Martin, M. Retention theory of sedimentation field-flow fractionation at finite concentrations. *Anal. Chem.* **1994**, *66* (10), 1718−1730.

(24) Giddings, J. C. A new separation concept based on a coupling of concentration and flow nonuniformities. *Sep. Sci.* **1966**, *1*, 123−125.

(25) Giddings, J. C. Field-flow fractionation: Analysis of macromolecular, colloidal, and particulate materials. *Science* **1993**, *260* (5113), 1456−1465.

(26) Kim, S. T.; Kang, D. Y.; Lee, S.; Kim, W. S.; Lee, J. T.; Cho, H. S.; Kim, S. H. Separation and quantitation of silver nanoparticles using sedimentation field-flow fractionation. *Journal of Liquid Chromatography and Related Technologies* **2007**, *30* (17), 2533−2544.

(27) Benincasa, M. A.; Giddings, J. C. Separation and molecular weight distribution of anionic and cationic water-soluble polymers by flow field-flow fractionation. *Anal. Chem.* **1992**, *64* (7), 790−798.

(28) Ratanathanawongs, S. K.; Shiundu, P. M.; Giddings, J. C. Size and compositional studies of core-shell latexes using flow and thermal field-flow fractionation. *Colloids Surf., A* **1995**, *105* (2−3), 243−250.

(29) Barman, B. N.; Ashwood, E. R.; Giddings, J. C. Separation and size distribution of red blood cells of diverse size, shape, and origin by flow/hyperlayer field-flow fractionation. *Anal. Biochem.* **1993**, *212* (1), 35−42.

(30) Zhang, J.; William, P. S.; Myers, M. N.; Giddings, J. C. Separation of cells and cell-sized particles by continuous SPLITT fractionation using hydrodynamic lift forces. *Sep. Sci. Technol.* **1994**, *29* (18), 2493−2522.

(31) Yang, F. J.; Myers, M. N.; Giddings, J. C. High-resolution particle separations by sedimentation field-flow fractionation. *J. Colloid Interface Sci.* **1977**, *60* (3), 574−577.

(32) Giddings, J. C.; Yang, F. J. F.; Myers, M. N. Application of sedimentation field-flow fractionation to biological partilces: molecular weights and separation. *Sep. Sci.* **1975**, *10* (2), 133−149.

(33) Giddings, J. C.; Myers, M. N.; Yang, F. J. F.; Smith, L. K. Mass analysis of particles and macromolecules by field-flow fractionation. In *Colloid and Interface Science*, Kerker, M., Ed.; Academic Press: New York, 1976; Vol. *IV*, pp 381−398.

(34) Giddings, J. C.; Myers, M. N.; Moellmer, J. F. Fine-particle separation and characterization by field-flow fractionation. *J. Chromatogr., A* **1978**, *149* (C), 501−517.

(35) Giddings, J. C.; Karaiskakis, G.; Caldwell, K. D.; Myers, M. N. Colloid characterization by sedimentation field-flow fractionation. I. Monodisperse populations. *J. Colloid Interface Sci.* **1983**, *92* (1), 66−80.

(36) Yang, F. S.; Caldwell, K. D.; Giddings, J. C. Colloid characterization by sedimentation field-flow fractionation. II. Particle-size distribution. *J. Colloid Interface Sci.* **1983**, *92* (1), 81−91.

(37) Giddings, J. C.; Yang, F. S. Colloid characterization by sedimentation field-flow fractionation. IV. Reinjection field-flow fractionation for polydisperse systems. *J. Colloid Interface Sci.* **1985**, *105* (1), 55−64.

(38) Jones, H. K.; Phelan, K.; Myers, M. N.; Giddings, J. C. Colloid characterization by sedimentation field-flow fractionation. V. Split outlet system for complex colloids of mixed density. *J. Colloid Interface Sci.* **1987**, *120* (1), 140−152.

(39) Giddings, J. C.; Yang, F. J. F.; Myers, M. N. Sedimentation field-flow fractionation. *Anal. Chem.* **1974**, *46* (13), 1917−1924.

(40) Giddings, J. C. Displacement and dispersion of particles of finite size in flow channels with lateral forces. field-flow fractionation and hydrodynamic chromatography. *Sep. Sci. Technol.* **1978**, *13* (3), 241−254.

(41) Williams, P. S.; Giddings, J. C. Theory of field-programmed field-flow fractionation with corrections for steric effects. *Anal. Chem.* **1994**, *66* (23), 4215−4228.
(42) Giddings, J. C. Nonequilibrium theory of field-flow fractionation. *J. Chem. Phys.* **1968**, *49* (1), 81−85.
(43) Van Den Broeck, C.; Maes, D. Retention and peak width in field-flow fractionation with wall effects. *Sep. Sci. Technol.* **1987**, *22* (4), 1269−1280.
(44) Hoshino, T.; Suzuki, M.; Ysukawa, K.; Takeuchi, M. Effects of detergent on the elution profiles of latex beads in sedimentation field-flow fractionation. *J. Chromatogr., A* **1987**, *400* (C), 361−369.
(45) Giddings, J. C.; Chen, X.; Wahlund, K. G.; Myers, M. N. Fast particle separation by flow/steric field-flow fractionation. *Anal. Chem.* **1987**, *59* (15), 1957−1962.
(46) Williams, P. S. K., X.; Giddings, J. C. *Chem. Eng. Commun.* **1992**, *111*, 121−147.
(47) Williams, P. S.; Lee, S.; Giddings, J. C. Characterization of hydrodynamic lift forces by field-flow fractionation. Inertial and near-wall lift forces. *Chem. Eng. Commun.* **1994**, *130*, 143−166.
(48) Hansen, M. E.; Giddings, J. C. Retention perturbations due to particle-wall interactions in sedimentation field-flow fractionation. *Anal. Chem.* **1989**, *61* (8), 811−819.
(49) Williams, P. S.; Xu, Y.; Reschiglian, P.; Giddings, J. C. Colloid characterization by sedimentation field-flow fractionation: correction for particle - wall interaction. *Anal. Chem.* **1997**, *69* (3), 349−360.
(50) Mori, Y.; Kimura, K.; Tanigaki, M. Influence of particle-wall and particle-particle interactions on retention behavior in sedimentation field-flow fractionation. *Anal. Chem.* **1990**, *62* (24), 2668−2672.
(51) Williams, P. S.; Moon, M. H.; Giddings, J. C. Influence of accumulation wall and carrier solution composition on lift force in sedimentation/steric field-flow fractionation. *Colloids Surf., A* **1996**, *113* (3), 215−228.
(52) Contado, C.; Bregola, L.; Dondi, F. Sedimentation field flow fractionation of immunoglobulin A coated polystyrene beads. Influence of carrier composition on complex characterization. *J. Chromatogr., A* **2007**, *1169* (1−2), 158−174.
(53) Beckett, R.; Ho, J.; Jiang, Y.; Giddings, J. C. Measurement of mass and thickness of adsorbed films on colloidal particles by sedimentation field-flow fractionation. *Langmuir* **1991**, *7* (10), 2040−2047.